

PAPER • OPEN ACCESS

An efficient and directional optical Tamm state assisted plasmonic nanolaser with broad tuning range

To cite this article: Zabir Ahmed and Muhammad Anisuzzaman Talukder 2018 *J. Phys. Commun.* **2** 045016

View the [article online](#) for updates and enhancements.

Related content

- [Semiconductor plasmonic nanolasers: current status and perspectives](#)
Shangjr Gwo and Chih-Kang Shih
- [Roadmap on plasmonics](#)
Mark I Stockman, Katrin Kneipp, Sergey I Bozhevolnyi et al.
- [Nanostructure arrays in free-space: optical properties and applications](#)
Stéphane Collin



PAPER

An efficient and directional optical Tamm state assisted plasmonic nanolaser with broad tuning range

OPEN ACCESS

RECEIVED

20 June 2017

REVISED

24 February 2018

ACCEPTED FOR PUBLICATION

19 March 2018

PUBLISHED

10 April 2018

Original content from this work may be used under the terms of the [Creative Commons Attribution 3.0 licence](#).

Any further distribution of this work must maintain attribution to the author(s) and the title of the work, journal citation and DOI.

Zabir Ahmed¹ and Muhammad Anisuzzaman Talukder^{1,2} ¹ Department of Electrical and Electronic Engineering Bangladesh University of Engineering and Technology, Dhaka 1205, Bangladesh² School of Electronic and Electrical Engineering University of Leeds, Leeds LS2 9JT, United Kingdom anis@eee.buet.ac.bd**Keywords:** plasmonic nanolaser, optical Tamm state, extraordinary optical transmission**Abstract**

In recent years, nanolasers based on plasmonic crystal nanocavity structures have attracted significant interest. However, the performance of such lasers is affected significantly by the coupling of the lasing emission to both reflection and transmission sides of the device and to multiple spatial modes in the far field due to higher-order diffraction from plasmonic crystals as well. In this work, we propose a nanolaser design that overcomes the performance degradation of plasmonic crystal based nanolasers and increases the emission intensity significantly. In the proposed nanolaser structure, a nanometer-thick gain medium has a one-dimensional photonic crystal on one side and a metal nanohole array on the other side. An incident pump pulse through the one-dimensional photonic crystal excites optical Tamm states at the metal-gain medium interface that are amplified by the stimulated emission of the gain medium. We find that the intensity of the extraordinary optical transmission through the metal nanohole array increases significantly due to the excitation of optical Tamm states with wavevector perpendicular to the nanohole array surface. We also find that the subwavelength periodicity in the nanohole array confines the lasing emission to the zero-th order mode only, and hence, makes the far-field pattern highly directional. Moreover, the laser emission wavelength can be tuned over a broad range by changing the thicknesses of the photonic crystal layers, gain medium, and in real-time, by changing the angle of incidence of the pump pulse.

1. Introduction

Nanoscale manipulation of light has led to drastic miniaturization of many optical devices such as bio-sensors, solar cells, and photodetectors. In many applications that use integrated optical systems such as optical interconnects, on-chip optical computing, bio-sensing, and non-linear optical applications, a nanoscale laser source is often required. Conventional lasers employing macroscopic photonic cavities are diffraction limited so that they cannot be smaller than half of the wavelength of operation [1]. To overcome this limit, novel waveguiding mechanisms capable of coupling electromagnetic energy within subwavelength dimensions are being explored [2, 3]. Plasmonic modes—surface plasmon polariton (SPP) and localized surface plasmon (LSP)—can confine electromagnetic energy beyond the diffraction limit, which makes them a promising choice for designing lasers with nanoscale dimensions. The first nanoscale laser using plasmonic structures was demonstrated in 2007 [4], and since then, a number of such nanolasers have been proposed and demonstrated both in visible and near infrared wavelength regimes utilizing structures that couple light to SPP modes [5–8] and hybrid photonic-plasmonic modes [2, 9, 10].

While SPP modes help to confine light in nanolasers, inherent ohmic losses associated with them limit the performance of such lasers. Additionally, scattering losses induced by surface roughness at the interfaces of the gain medium and plasmonic structures affect the lasing emission. The ohmic and scattering losses in plasmonic structures make it inevitable for the nanolasers to operate at cryogenic temperature and have an active medium with high gain [11, 12]. Another fundamental drawback of nanolasers based on SPP mode excitation is the divergent far-field radiation due to a large mismatch between the wavevectors of light in plasmonic modes and in

free-space radiative modes. In recent years, nanolasers based on plasmonic crystals—structures consisting of periodic arrangement of metal nanoparticles—have been demonstrated to achieve directional emission [13]. Periodic array of nanoparticles can excite band-edge lattice plasmon modes, which can produce narrow-beam emission via in-phase interference between the emission patterns of nanoparticles. Plasmonic nanolasers based on lattice plasmon modes have been reported to emit a strong spatially coherent light with a divergence angle of $\lesssim 1.5^\circ$. The band-edge lattice plasmon modes also exhibit reduced radiative losses, and thus result in increased laser emission intensity. The radiative losses, and hence, the lasing threshold in plasmonic lasers can be further reduced by exploiting optical Tamm states excited using a photonic crystal [14, 15].

Plasmonic structures consisting of periodic nanohole arrays covered by gain medium have also been demonstrated to produce stimulated emission [16–18]. Periodic nanohole arrays can couple light to SPP-Bloch modes and exhibit resonant transmission known as extraordinary optical transmission (EOT) [19]. The stimulated emission from the gain medium couples to resonant SPP-Bloch modes resulting in amplification and lasing, and a highly directional far-field emission profile. At visible wavelength, such metal hole array based lasers have produced far-field emission profiles with a divergence angle of $\sim 1\text{--}3^\circ$ [20].

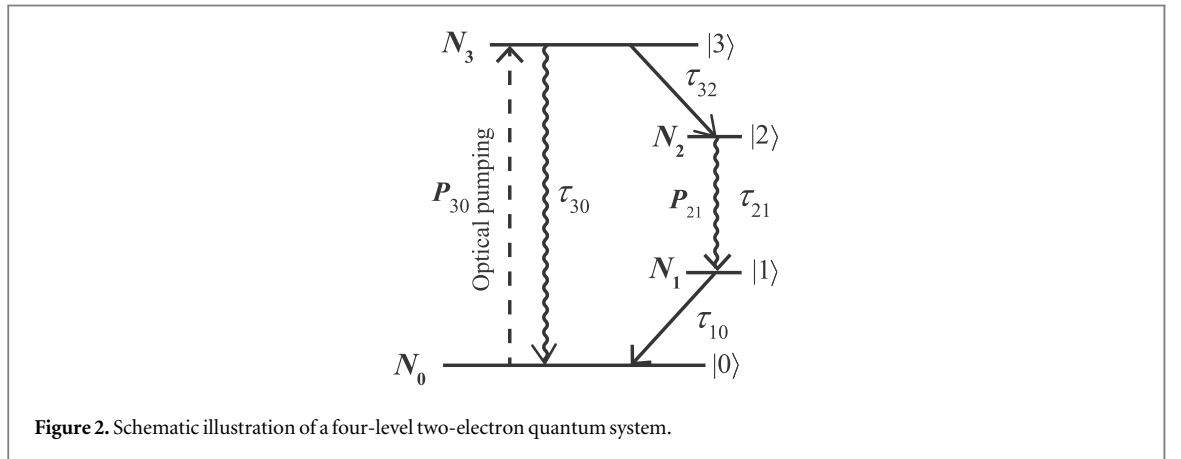
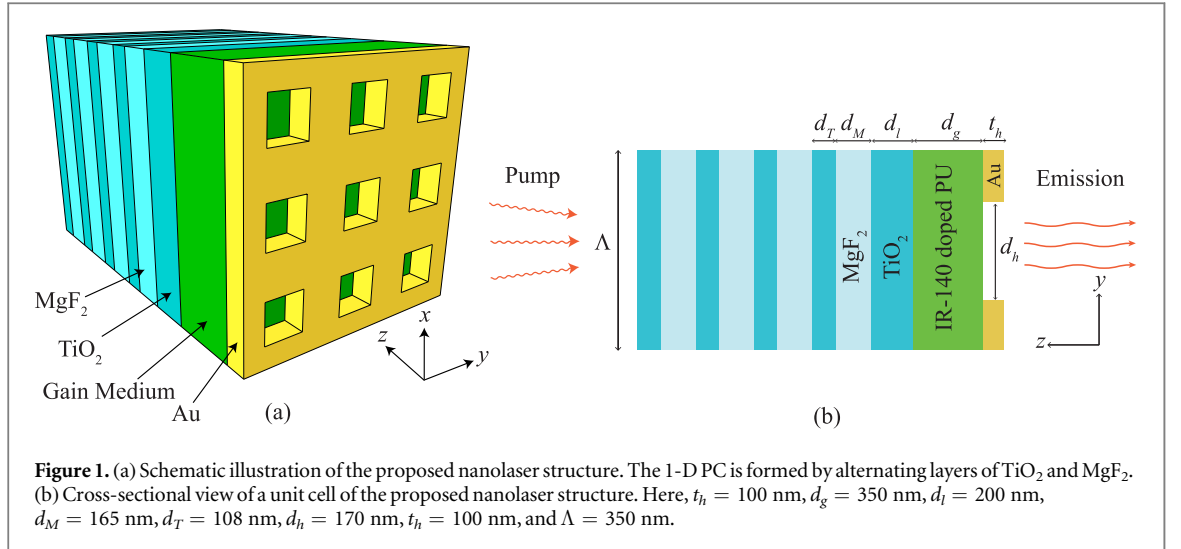
While plasmonic crystal based nanolasers can produce directional emission, the emission energy of such lasers is affected significantly mainly due to two reasons. Firstly, since the lattice period of the metal nanoparticle array is close to the operating wavelength of the laser, structures support multiple diffracted modes at lasing wavelength [13, 20, 21]. Therefore, the total emission intensity is distributed among multiple far-field off-normal spatial modes in addition to the fundamental lasing mode in the normal direction, which results in reduced emission intensity of the fundamental lasing mode. Secondly, lasing emission is observed from both top and bottom surfaces. Therefore, the emitted energy is distributed in a number of diffracted modes at a number of angles from both top and bottom surfaces. As a result, the emission intensity of the fundamental lasing mode is affected significantly. Recently, unidirectional lasing has been achieved using template-stripped two-dimensional plasmonic crystals, where optically thick gold (Au) substrate reflects lasing emission onto the same side as the pump source [22]. However, such a structure suffers from the complexity related to separating the lasing emission from the incident light, increased ohmic losses in the metal layer, and lack of far-field directionality of lasing emission.

Broadband tunability of nanoscale lasers promises numerous potential applications. There have been recent demonstrations of wavelength-tunable SPP based nanolasers by changing the composition of gain medium [23]. Wavelength tuning over 65 nm in visible wavelength regime by changing the doping level in organic gain medium has also been reported [20]. In plasmonic crystal based nanolasers, real-time wavelength tuning over 55 nm has been demonstrated by changing the refractive index of liquid gain medium through microfluidic arrangements [21].

In this paper, we propose a plasmonic nanolaser that is capable of lasing at room temperature in near-infrared regime with the peak emission at ~ 875 nm. In the proposed design, we use EOT and optical Tamm state (OTS) resonances to create optical feedback in the laser cavity. The proposed structure includes a one-dimensional (1-D) photonic crystal (PC) on the gain medium, which is placed on the top of a metal nanohole array (NHA) with subwavelength periodicity. The PC layers help the stimulated emission from the gain medium to couple to OTS modes at the interface between the metal layer and gain medium, which leads to enhanced plasmonic-photonic resonance in the nanocavity. Moreover, PC layers selectively guide the stimulated emission from the gain medium toward the transmission side, and thus result in increased lasing intensity. The subwavelength periodicity of the two-dimensional metal NHA limits the number of diffracted modes and produces a highly directional emission with a divergence angle of $\lesssim 1^\circ$. Additionally, the emission wavelength of the nanolaser can be changed by controlling the thicknesses of the PC layers and gain medium. The proposed nanolaser can also be tuned dynamically by changing the incident angle of the pump pulse.

2. Design and simulation

In figure 1(a), we present a three-dimensional schematic illustration of the proposed nanolaser structure. In figure 1(b), we show a cross-sectional view of a unit cell of the proposed structure in the y - z plane. The proposed structure has a subwavelength-thick gain medium placed on an Au layer perforated with a periodic square NHA. The gain medium consists of dye molecules IR-140 embedded in Polyurethane (PU). IR-140 molecules have an absorption peak at 800 nm and an emission peak at 870 nm. The gain medium has a 1-D PC on the top that consists of alternating layers of titanium oxide (TiO_2) and magnesium fluoride (MgF_2). We denote the number of pairs of TiO_2 - MgF_2 layers in PC by N . We also denote the TiO_2 and MgF_2 layer thicknesses by d_T and d_M , respectively. The terminating TiO_2 layer that connects the PC structure to the laser gain medium has a different thickness compared to the TiO_2 layers in the PC. The nanohole width and the thickness of the Au layer are denoted by d_h and t_h , respectively.



We have studied the dynamics of the proposed structure when a resonant pump pulse is incident into the gain medium through the PC as shown in figure 1(b). Absorption and fluorescence processes of the dye molecules in the gain medium take place between four energy levels in a singlet manifold. Therefore, dye lasers can be modeled as a four-level system [24]. In this work, we have modeled IR-140 using a semi-quantum mechanical framework applied to a four-level two-electron system [25]. In this framework, although IR-140 is modeled as a four-level quantum system, the electromagnetic field is modeled classically. In figure 2, we show a schematic illustration of the four-level system that we used to model the gain medium. A pump pulse that is resonant to the energy difference between levels $|0\rangle$ and $|3\rangle$ is incident to excite population density from level $|0\rangle$ to level $|3\rangle$. The population density of the excited level $|3\rangle$ decays fast to level $|2\rangle$ non-radiatively. Radiative transition between levels $|2\rangle$ and $|1\rangle$ leads to lasing emission if there is population inversion between these two levels. Population density of level $|1\rangle$ relaxes fast to level $|0\rangle$ by non-radiative transitions.

The radiative transitions in this four-level system can be treated as two coupled dipole oscillators. Levels 0 and 3 are coupled by dipole \vec{P}_{30} with a dephasing rate γ_{30} , whereas, levels 1 and 2 are coupled by dipole \vec{P}_{21} with a dephasing rate γ_{21} . The equations that govern the dynamics of polarization densities are given by [26]

$$\frac{d^2\vec{P}_{30}}{dt^2} + \gamma_{30}\frac{d\vec{P}_{30}}{dt} + \omega_{30}^2\vec{P}_{30} = \frac{6\pi\epsilon_0c^3}{\omega_{30}\tau_{30}}(N_3 - N_0)\vec{E}, \quad (1a)$$

$$\frac{d^2\vec{P}_{21}}{dt^2} + \gamma_{21}\frac{d\vec{P}_{21}}{dt} + \omega_{21}^2\vec{P}_{21} = \frac{6\pi\epsilon_0c^3}{\omega_{21}\tau_{21}}(N_2 - N_1)\vec{E}. \quad (1b)$$

In equation (1), N_i is the population density probability in level i , ω_{ij} is the transition frequency between levels i and j , τ_{ij} is the decay time constant between levels i and j , ϵ_0 is the free-space permittivity, and c is the speed of light in vacuum.

Population densities of different levels of the gain medium are governed by the coupled rate equations given by [26]

Table 1. Refractive indices of dielectric layers.

| Material | Refractive Index |
|------------------|------------------|
| TiO ₂ | 2.23 |
| MgF ₂ | 1.38 |
| PU | 1.51 |

$$\frac{dN_3}{dt} = -\frac{N_3(1 - N_2)}{\tau_{32}} - \frac{N_3(1 - N_0)}{\tau_{30}} + \frac{1}{\hbar\omega_{30}} \vec{E} \cdot \frac{d\vec{P}_{30}}{dt}, \quad (2a)$$

$$\frac{dN_2}{dt} = \frac{N_3(1 - N_2)}{\tau_{32}} - \frac{N_2(1 - N_1)}{\tau_{21}} + \frac{1}{\hbar\omega_{21}} \vec{E} \cdot \frac{d\vec{P}_{21}}{dt}, \quad (2b)$$

$$\frac{dN_1}{dt} = \frac{N_2(1 - N_1)}{\tau_{21}} - \frac{N_1(1 - N_0)}{\tau_{10}} - \frac{1}{\hbar\omega_{21}} \vec{E} \cdot \frac{d\vec{P}_{21}}{dt}, \quad (2c)$$

$$\frac{dN_0}{dt} = \frac{N_3(1 - N_0)}{\tau_{30}} + \frac{N_1(1 - N_0)}{\tau_{10}} - \frac{1}{\hbar\omega_{30}} \vec{E} \cdot \frac{d\vec{P}_{30}}{dt}. \quad (2d)$$

The equations (1) and (2) are coupled to Maxwell-Ampere's law given by [26]

$$\frac{d\vec{E}}{dt} = \frac{1}{\epsilon} \nabla \times \vec{H} - \frac{1}{\epsilon} N_i \left(\frac{d\vec{P}_{30}}{dt} + \frac{d\vec{P}_{21}}{dt} \right), \quad (3)$$

where ϵ is the permittivity of the material, and \vec{E} and \vec{H} are the electric and magnetic fields, respectively. Equations (1)–(3) provide us with a set of self-consistent equations, which are numerically solved to calculate the time-resolved dynamics of the gain medium in response to the optical pumping.

We have numerically solved equations (1)–(3) for the proposed structure using a full-field vectorial electromagnetic simulator Lumerical FDTD Solutions. In numerical simulation, the proposed nanolaser structure was assumed to be infinitely periodic in the x - and y -directions. Therefore, periodic Bloch boundary condition was chosen in both the x - and y -directions. Perfectly matched layers (PML) were used on the z -boundaries. Due to the periodicity of the structure in the x - and y -directions, we only simulated a single unit cell of the structure with a periodicity $\Lambda = 350$ nm in the x - and y -directions to calculate the response of the entire structure. We chose the lattice period of the NHA to be subwavelength so that only the zero-th order of the diffracted modes exists for lasing emission. For optical pumping, we used a Gaussian pulse with a duration of 40 fs, which was centered at 800 nm wavelength with a linewidth of 20 nm. We placed a frequency domain field monitor at the near field on the emission side to record the lasing emission. We calculated the emission characteristics at different wavelengths by integrating the poynting vectors normal to this field monitor.

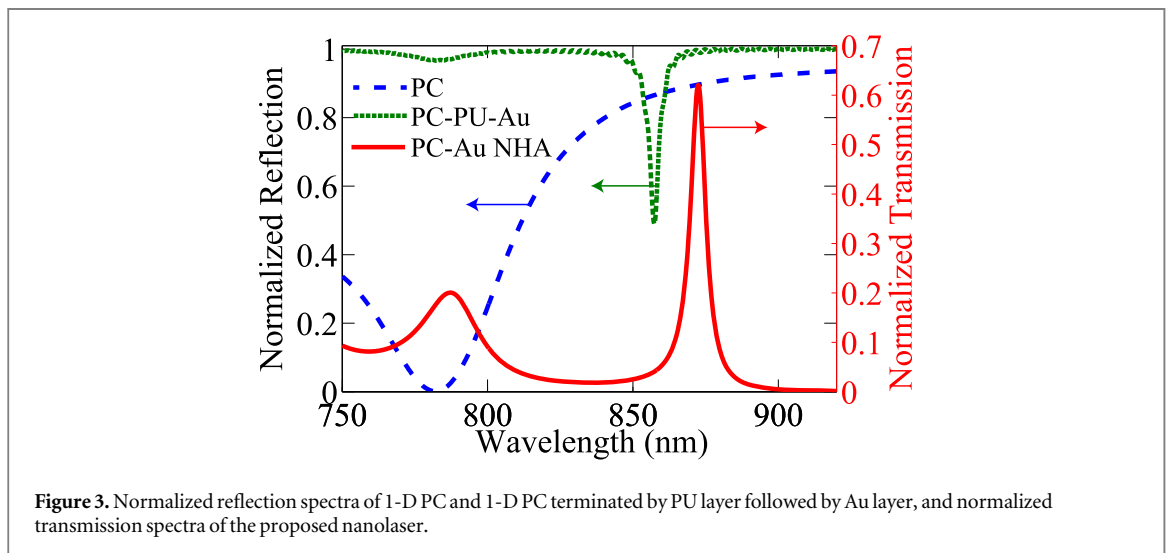
The electromagnetic simulator uses a multi-coefficient model to account for the dispersive nature of Au in near-infrared regime. The optical parameter of Au was taken from Johnson and Christy [27]. The dielectric materials in the proposed structure were assumed to be non-dispersive in the near-infrared regime. The refractive indices of the dielectric materials in the proposed structure are given in table 1 [28]. Since IR-140 is embedded in PU, the base refractive index of the gain material was chosen to be that of PU. We have designed the proposed laser for room-temperature operation. IR-140 gain medium is especially used in plasmonic lasers for its ability to produce high gain to compensate the ohmic losses in metal. A fully inverted IR-140 gain medium with a population density of only $6 \times 10^{17} \text{ cm}^{-3}$ has been theoretically predicted to produce a gain of $\sim 360 \text{ cm}^{-1}$ [12, 29]. IR-140 gain medium has been used in similar plasmonic nanolasers and has been found to produce lasing emission by overcoming the losses in plasmonic structures [13, 15, 22]. We have used parameter values for IR-140 gain medium from [13] as given in table 2. The parameter values for IR-140 gain medium have been found to match well with experimental findings.

3. Cavity dynamics

In the proposed nanolaser, the resonant cavity is formed by an Au NHA in one side of the gain medium and a 1-D PC on the other side of the gain medium. The stimulated emission from the gain medium couples to localized resonances in nanoholes and is transmitted through the perforated metal layer by EOT mechanism [30, 31]. The 1-D PC on top of the gain medium helps the stimulated emission to excite OTS modes, and thus leads to high intensity field distribution in the vicinity of the interface between the metal layer and gain medium. The field enhancement due to OTS consequently results in enhanced EOT through the nanoholes [32]. In figure 3, we show normalized reflection spectra for a bare 1-D PC and for a 1-D PC terminated by a PU layer

Table 2. Parameter values for IR-140 dye molecules.

| Parameter | Value |
|---|------------------------------------|
| Absorption wavelength (λ_{30}) | 800 nm |
| Absorption linewidth ($\Delta\lambda_{30}$) | 100 nm |
| Emission wavelength (λ_{21}) | 870 nm |
| Emission linewidth ($\Delta\lambda_{21}$) | 100 nm |
| Transition lifetimes $\tau_{21} = \tau_{30}$ | 1 ns |
| $\tau_{32} = \tau_{10}$ | 10 fs |
| Dye concentration | $2 \times 10^{18} \text{ cm}^{-3}$ |

**Figure 3.** Normalized reflection spectra of 1-D PC and 1-D PC terminated by PU layer followed by Au layer, and normalized transmission spectra of the proposed nanolaser.

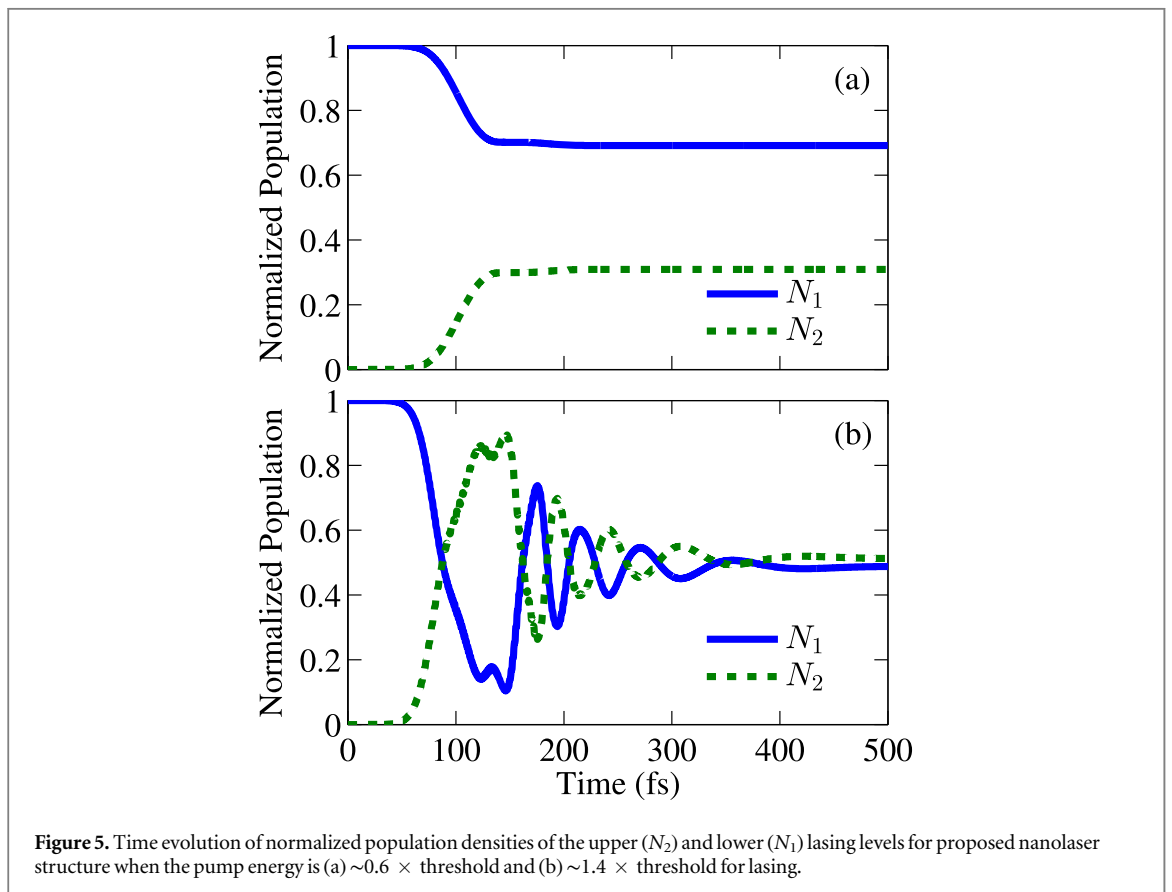
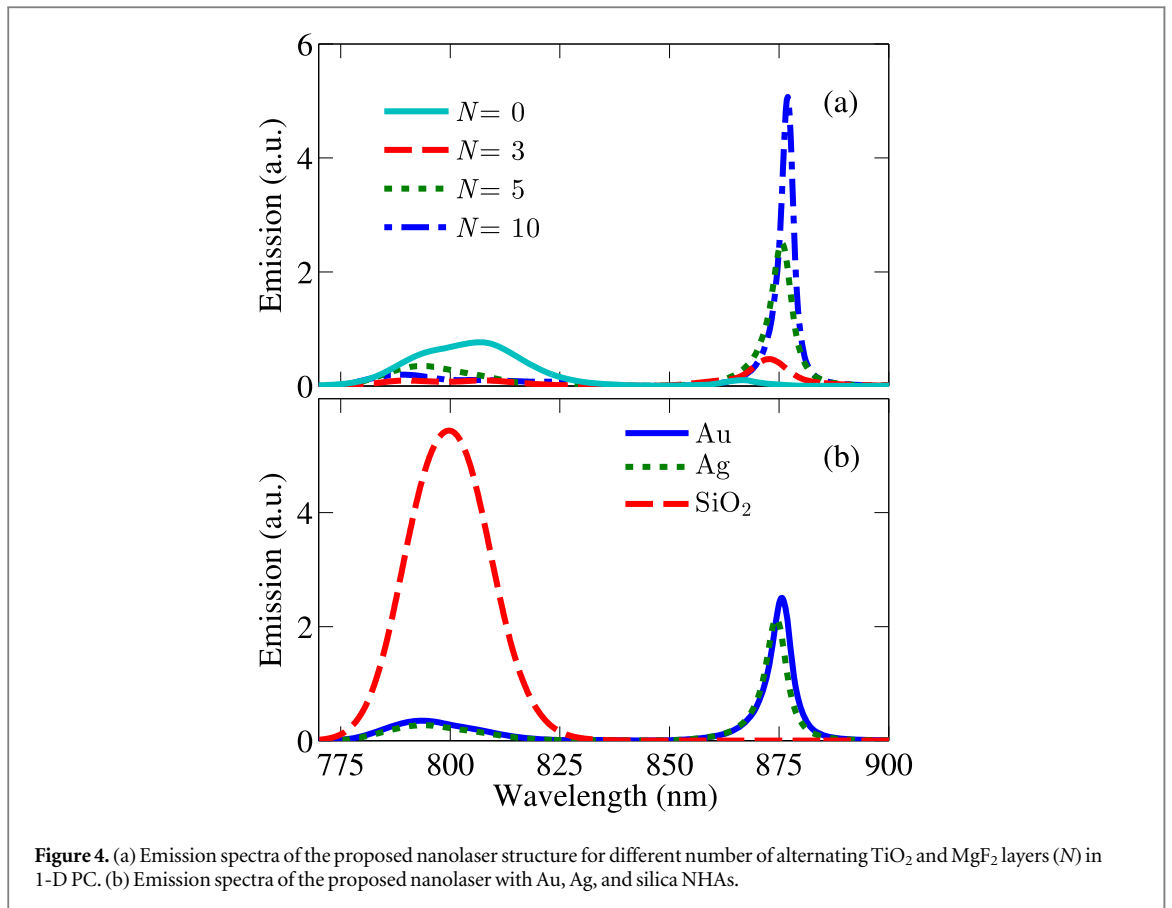
followed by a solid Au layer. At ~ 857 nm, a reflection minimum is observed for PC-PU-Au structure, which corresponds to the OTS resonance. We note that the OTS resonance resides within the stop-band regime of the bare PC structure. The resonant wavelength of OTS depends on the PU and PC layers thicknesses [33]. Theoretically, we can calculate the resonant wavelength for OTS using the condition [34]

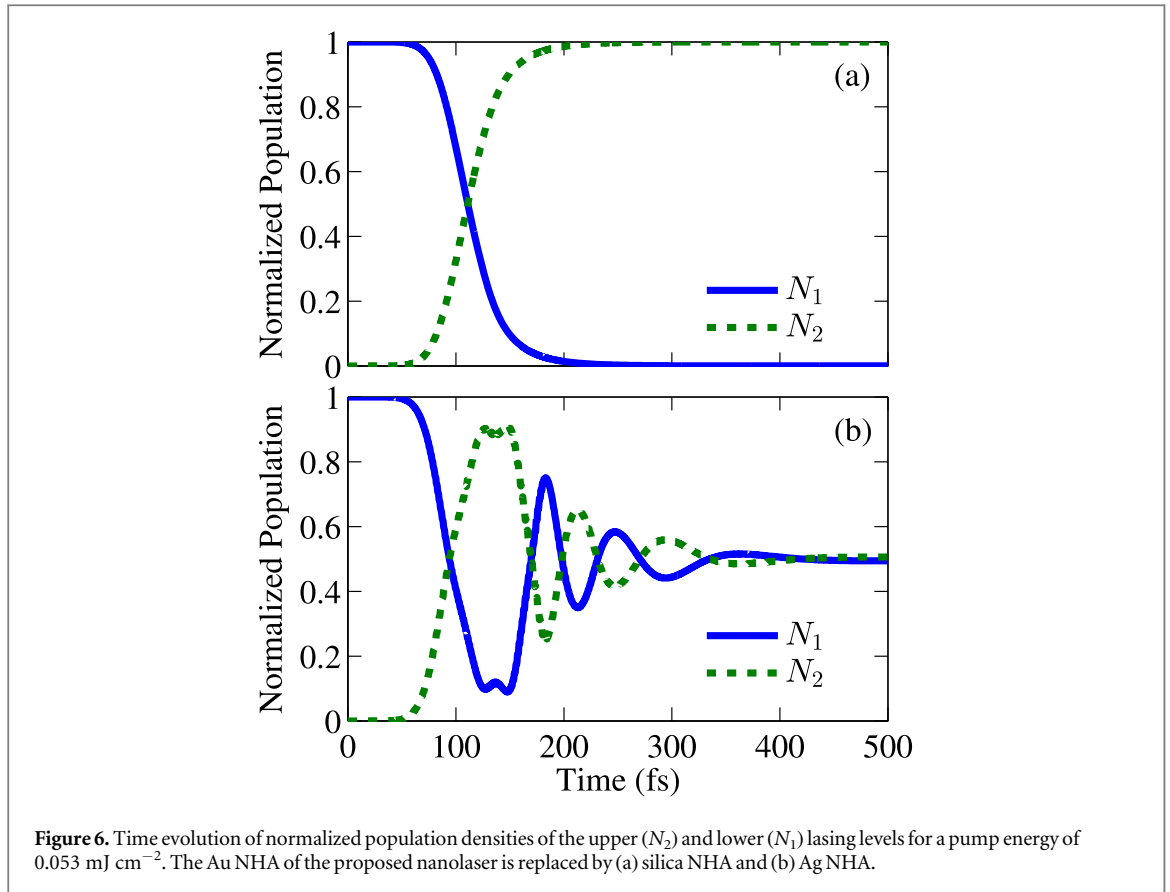
$$r_{\text{PC}} r_{\text{AuPU}} e^{(2i\phi)} = 1, \quad (4)$$

where r_{AuPU} is the amplitude reflection coefficient for incidence from Au to PU, r_{PC} is the amplitude reflection coefficient for wave incident from a medium with refractive index of TiO_2 on the PC starting with TiO_2 , and $\phi = 1.51 \times d_g \times \omega/c$ is the phase shift of the wave with angular frequency ω propagating in the PU layer of thickness d_g . Figure 3 also shows the normalized transmission spectra of the proposed nanolaser cavity with 1-D PC on top of Au NHA. We note enhanced EOT assisted by OTS resonance at 872 nm wavelength. From numerical simulations, we chose the thicknesses of PU and PC layers of the proposed nanolaser for resonant transmission around the peak photoluminescence wavelength ~ 870 nm of the gain medium for optimal lasing emission.

To investigate the effect of 1-D PC to improve the emission characteristic of the proposed nanolaser, we have calculated the emission spectra with varying number of pairs of MgF_2 - TiO_2 layers N . In figure 4(a), we show the change in the emission spectra when N changes from zero to 10. When there is no PC, i.e., $N = 0$, the gain medium is sandwiched between a 200-nm-thick TiO_2 layer and a 100-nm-thick metal hole array. We note that the emission intensity is low and the emission spectra is broad with a peak at ~ 860 nm when $N = 0$. However, as N increases, the emission intensity increases significantly. The emission intensity increases by more than an order of magnitude when N increases from zero to 10. Additionally, the emission shows increased spectral coherence with the increase of N as the linewidth narrows significantly. We also note that the scattered pump intensity at the output around 800 nm wavelength range decreases as N increases.

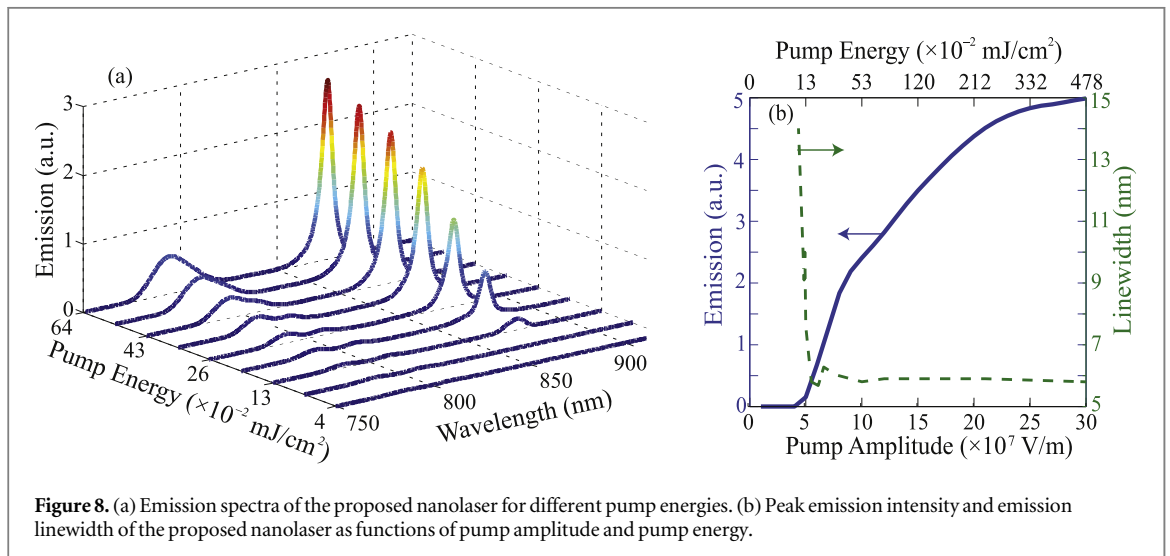
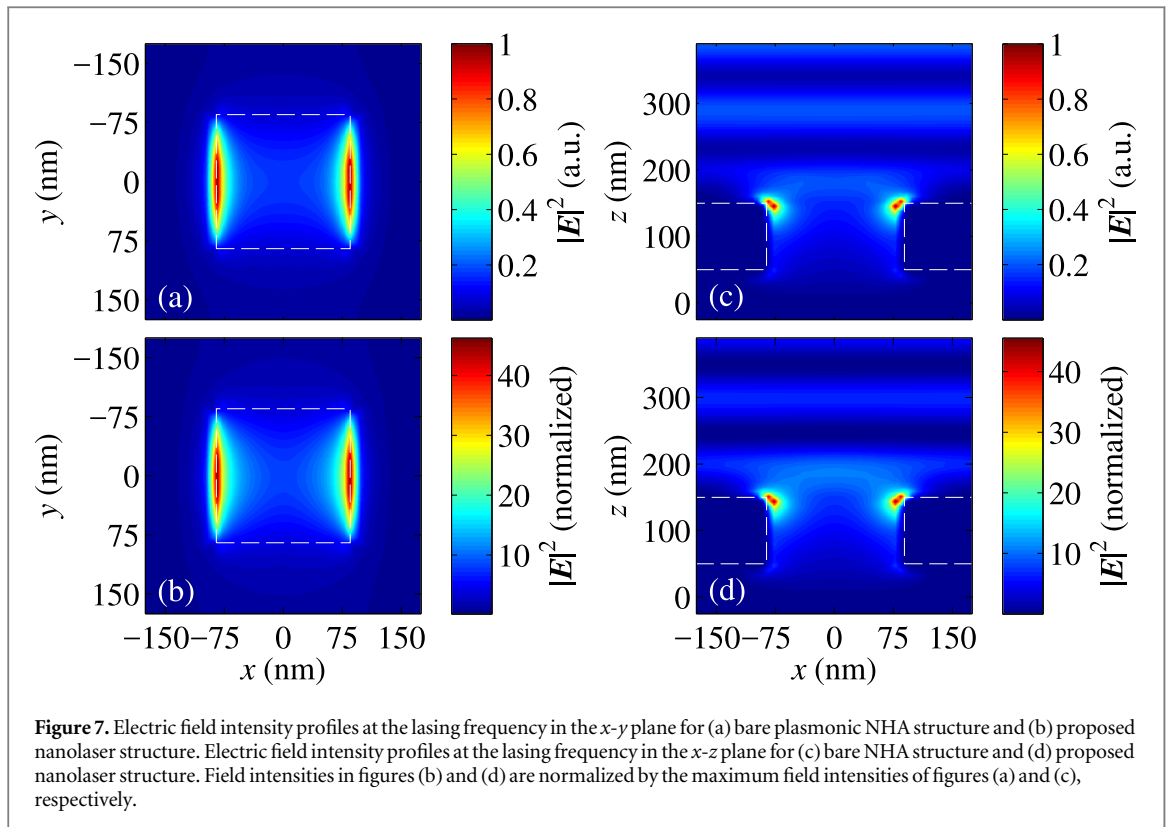
To illustrate the importance of plasmonic modes in the operation of the proposed nanolaser, we have simulated other structures where the Au NHA is replaced by SiO_2 and Ag NHAs. The optical parameter of Ag was taken from Palik [35]. The results are shown in figure 4(b). We observe lasing emission from the structures with Au and Ag NHAs, but not from the structure with Silica NHA. In figure 5, we plot the time resolved population densities of the two lasing levels after the pump pulse interacts with the gain medium in our proposed nanolaser structure with Au NHA. In figure 5(a), we show the change in population densities with time when the pump energy is $0.0085 \text{ mJ cm}^{-2}$, which is slightly less than the threshold for lasing. We note that the





lasing levels are not inverted with this pump energy. However, when the pump pulse has an energy of 0.019 mJ cm^{-2} , which is greater than the threshold required for lasing, we note that the lasing levels are inverted after the pump pulse interacts as shown in figure 5(b). When the Au NHA is replaced by a silica NHA of the same dimensions, we observe no lasing from the structure even when the pump energy is 36 times of the threshold value for our proposed structure. Upon further investigation of the population densities of the structure, we find that the gain medium reaches population inversion with a silica NHA when the pump pulse has an energy of 0.026 mJ cm^{-2} , but fails to support lasing emission as the silica NHA cannot provide sufficient feedback essential for lasing action. In figure 6(a), we show the population densities of the structure with silica NHA when the pump pulse has an energy of 0.053 mJ cm^{-2} . Although, we note population inversion between the lasing levels after the pump pulse interacts, we do not observe any lasing in the emission spectra of the structure with silica NHA. However, when the Au NHA is replaced by an Ag NHA of the same dimensions, we observe lasing emission from the device. In a structure with an Ag NHA, plasmonic modes and OTS modes between Ag and the gain medium can provide the feedback action necessary for lasing emission. The time evolution of population densities for the lasing levels with an Ag NHA is shown in figure 6(b).

We have calculated the spatial electric field distribution in the laser structure to investigate the underlying mechanisms of lasing and the contribution of the 1-D PC to the performance of the proposed plasmonic nanolaser. Figures 7(a) and 7(b) show electric field intensity distributions in a unit cell of the nanolaser in the x - y plane at the interface between Au NHA and gain medium without the 1-D PC and with the 1-D PC, respectively. For bare NHA structure, we observe field enhancement at the sides of square holes due to excitation of LSP modes as shown in figure 7(a). In figure 7(b), the field profile along the same NHA-gain medium interface is shown for the structure with 1-D PC. While the mode profile is similar to that of the bare NHA structure, we observe ~ 50 times enhancement in the peak field intensity due to the inclusion of the PC structure. We attribute this enhancement to the coupling of the stimulated emission to OTS modes, and hence increased coupling to the plasmonic modes. Figures 7(c) and 7(d) show electric field intensity distributions in the x - z plane through the center of a nanohole without the 1-D PC and with the 1-D PC, respectively. We observe similar field enhancement and high confinement of modal profile with the 1-D PC in the x - z plane as well.

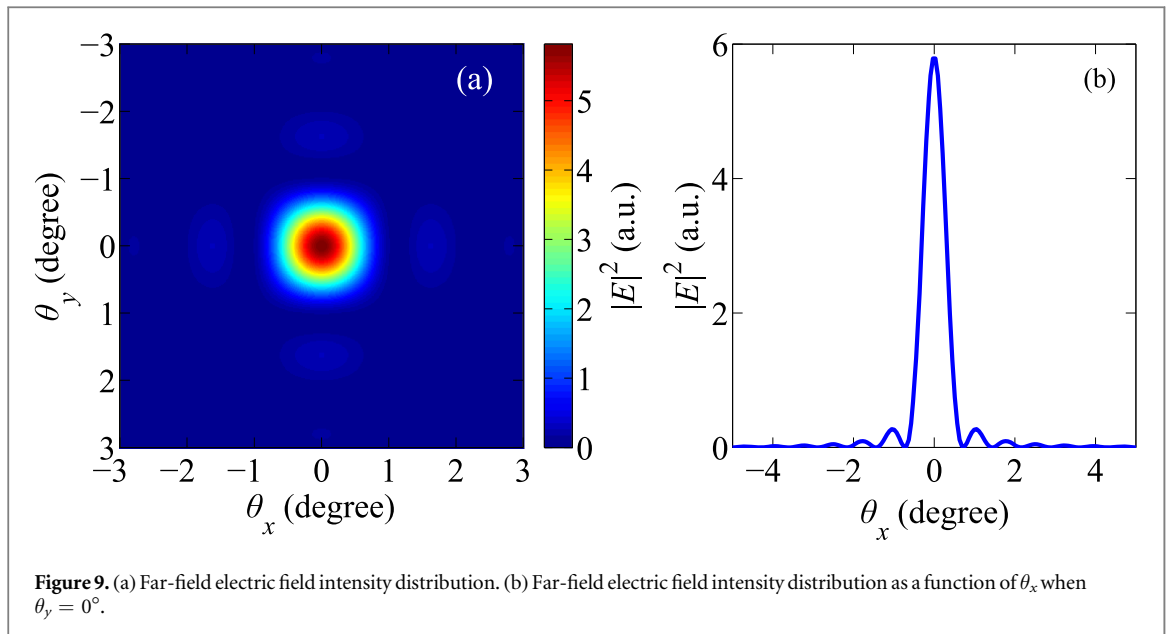


4. Emission characteristics

4.1. Lasing threshold and emission intensity

We have simulated the response of the proposed nanolaser structure under normally incident optical pumping for a range of pump energies. The calculated emission spectra are presented in figure 8(a). We find that there is negligible emission at the lasing wavelength when the pump energy is $< 0.013 \text{ mJ cm}^{-2}$. When the pump energy is $\geq 0.013 \text{ mJ cm}^{-2}$, we note the onset of lasing at $\sim 870 \text{ nm}$. We also observe that the linewidth of the stimulated emission spectra narrows as the pump energy increases.

In figure 8(b), we draw the peaks of lasing emission intensities and the linewidth of the emission spectra as functions of input pump amplitude and pump energy. We find that the laser reaches threshold when the pump pulse has an energy of $\sim 0.013 \text{ mJ cm}^{-2}$. As the pump energy increases beyond threshold, the lasing intensity increases sharply. However, for a pump energy of $> 0.332 \text{ mJ cm}^{-2}$, the lasing emission begins to saturate. We note that the emission linewidth decreases from $\sim 14 \text{ nm}$ to $\sim 5.8 \text{ nm}$ as the pump energy increases from threshold to 0.478 mJ cm^{-2} . We find that $\sim 34\%$ of the lasing mode intensity is lost mainly due to ohmic losses in



the metal structure. The emission from the proposed nanolaser can be justified as lasing by the narrowing of the emission linewidth, the requirement of threshold pump energy for lasing, and the gain saturation at high pump energy.

4.2. Far-field directionality

There is a huge difference in the wavevectors of light when it is coupled to SPP compared to when it propagates in free space. Therefore, when the confined light at the metal-gain medium interface of a plasmonic nanolaser radiates in free space, the phases of the propagating waves can be distorted and result in a diverging beam. However, in the proposed structure, lasing light is coupled to LSPs, which are confined in the holes of the metal NHA. Each of the square holes in the NHA with the confined light behaves like a dipole emitter radiating coherent spherical waves [32]. The radiated coherent spherical waves from the square holes interfere constructively in the far-field and create directional emission in the surface-normal direction.

We can achieve high spatial coherence from our proposed plasmonic NHA based nanolaser. We calculate the far-field profile by transforming the near-field profile obtained with a frequency domain field profile monitor placed at the near field on the emission side of the laser. For a periodic structure, the far-field pattern depends on the number of lattice periods in the structure. As the number of lattice period is increased, the far-field pattern becomes narrower. We have assumed that the proposed structure is $70 \mu\text{m}$ long in both the x - and y -directions and the pumping source is a ‘top-hat’ type. Therefore, in simulation, the proposed structure with an area of $70 \mu\text{m} \times 70 \mu\text{m}$ is uniformly illuminated by the pumping source. The far-field pattern is given in figure 9(a), where θ_x and θ_y denote the angles formed by the points of the far-field plane with the y - z and x - z planes, respectively. We find that the divergence angle of intensity distribution is small with a full-width at half-maximum of only $\sim 1^\circ$. In figure 9(b), we show a cross-sectional view of the far-field pattern along θ_x when $\theta_y = 0^\circ$. We note a narrow-beam emission profile, which is centered at $\theta_x = 0^\circ$. In theory, we can achieve even smaller divergence angle with increased number of lattice periods in the proposed structure. Figure 10 shows that the divergence angle decreases as the lengths of the nanolaser increase in the transverse directions. We find that the divergence angle can be as small as 0.3° when the proposed nanolaser has an area of $210 \mu\text{m} \times 210 \mu\text{m}$ in the x - y plane. However, in practice, the divergence angle of EOT through a periodic subwavelength NHA can be limited to $\sim 1^\circ$ due to imperfections and limitations related to fabrication processes [18].

In addition to the far-field profile, divergence property of the proposed nanolaser is studied by investigating the poynting vectors in the near field, which show the directions of energy flow. In figure 11(a), we show the magnitude of the poynting vectors, and in figures 11(b)–(d), we show the components of the poynting vectors in the x -, y -, and z -directions, respectively. We note that the component of the poynting vectors in the z -direction is four orders of magnitude greater than that in the x - and y -directions. Therefore, the resultant poynting vector is predominantly directed in the z -direction, i.e., toward normal to NHA surface, and results in a highly directional emission from the proposed nanolaser.

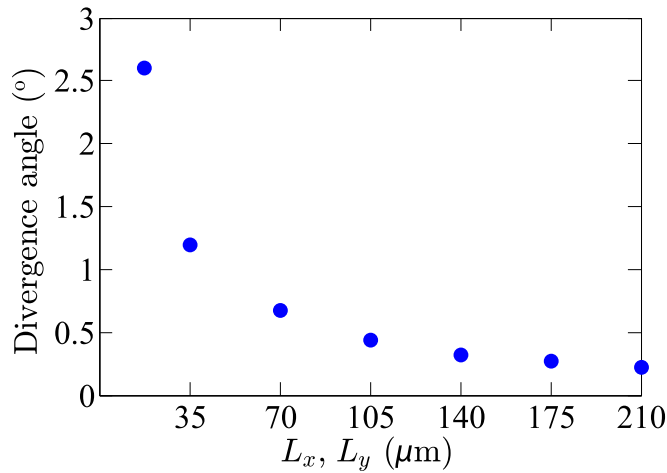


Figure 10. Divergence angle of far-field radiation with increasing length of the nanolaser in the x - (L_x) and y - directions (L_y).

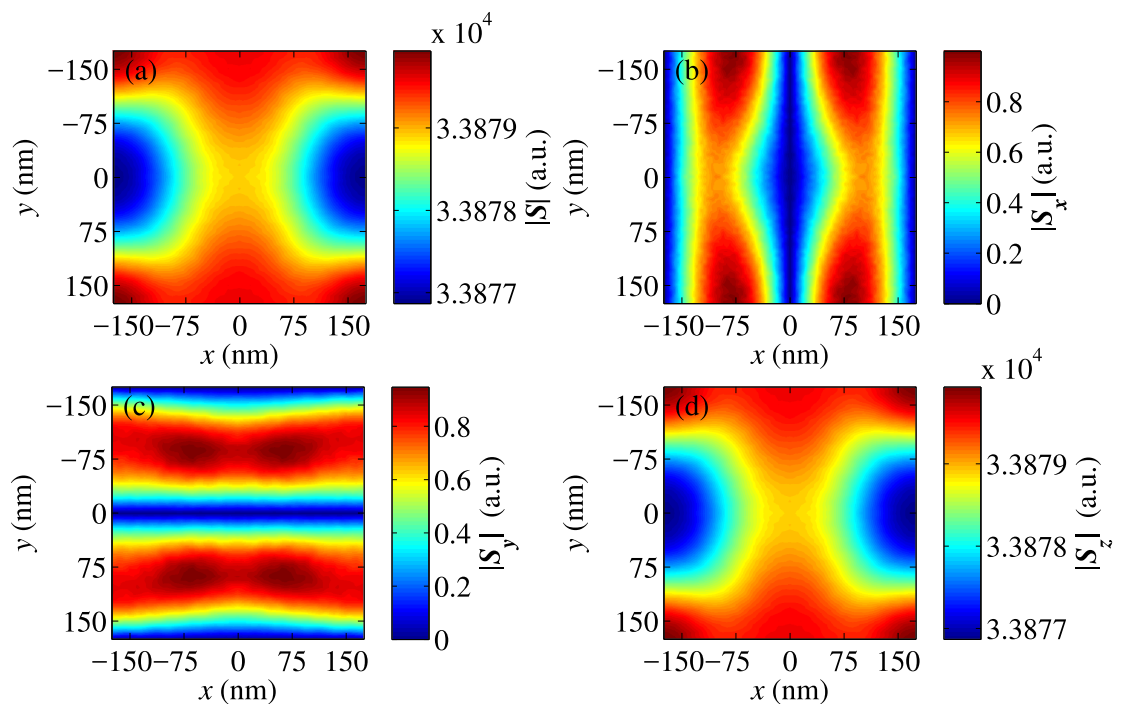


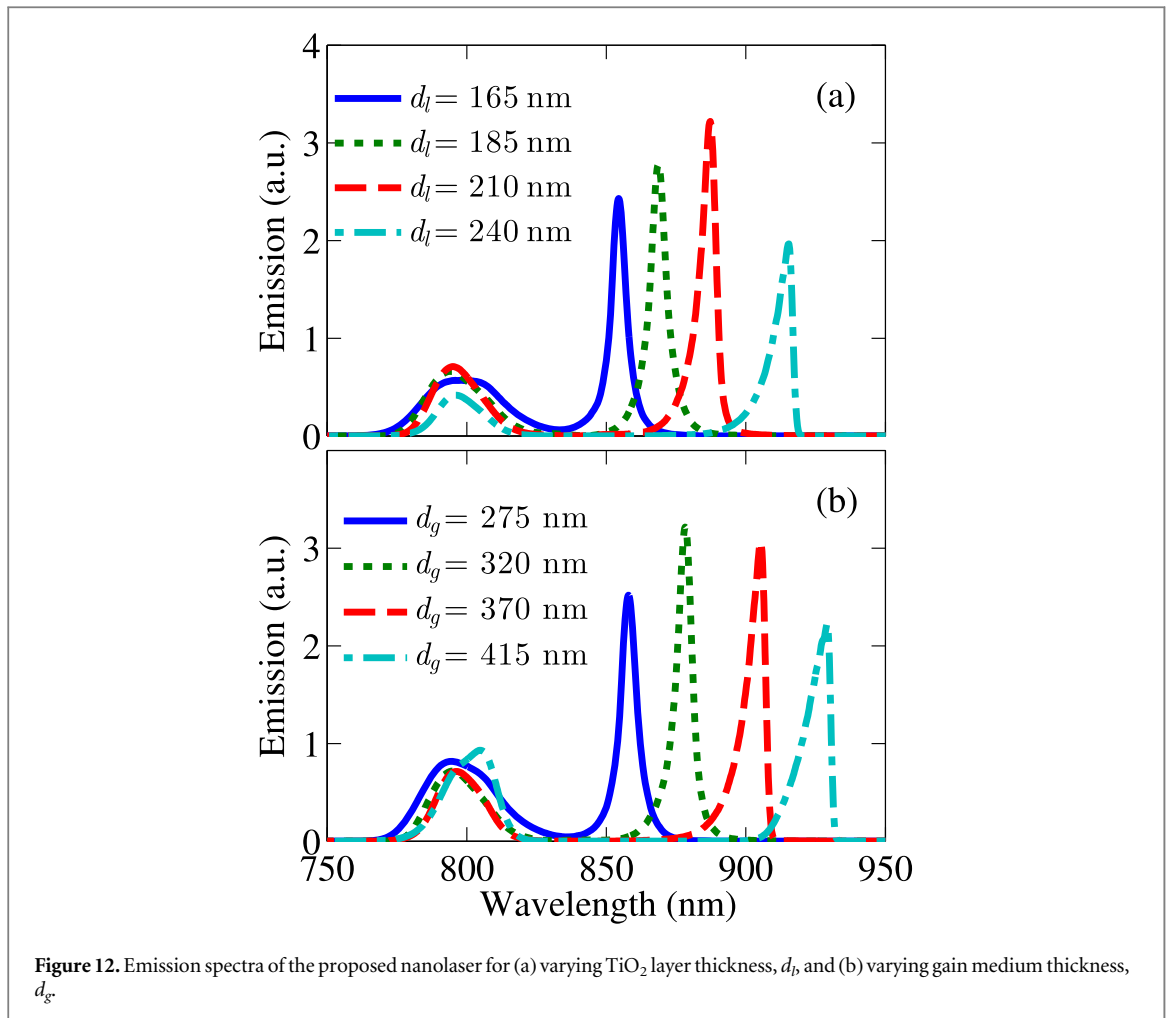
Figure 11. (a) Magnitude of resultant Poynting vector $|S|$ in the near field at lasing frequency. Orthogonal components of Poynting vector at lasing frequency (b) $|S_x|$, (c) $|S_y|$, and (d) $|S_z|$.

5. Tuning emission spectra

The emission wavelength of the proposed plasmonic nanolaser structure can be tuned in many ways. The resonance of OTS coupled between the 1-D PC and metal layer is sensitive to the thicknesses of the layers adjacent to the metal [33, 36]. We have exploited this property by changing the thicknesses of TiO_2 and gain layers to tune the emission wavelength of our proposed nanolaser over 60 nm. Additionally, we can dynamically tune the stimulated emission wavelength by changing the incident angle of the pump pulse.

5.1. Terminating TiO_2 layer thickness

In the proposed structure, we have varied the thickness of the terminating TiO_2 layer, d_t , and observed a significant shift of the lasing emission spectra. In particular, we found that the peak of the emission spectra varies from 855 nm to 920 nm when d_t is varied from 165 nm to 240 nm. The results are given in figure 12(a). We do not find lasing when $d_t < 140$ nm or $d_t > 250$ nm. We also observe that the peak emission intensity reaches



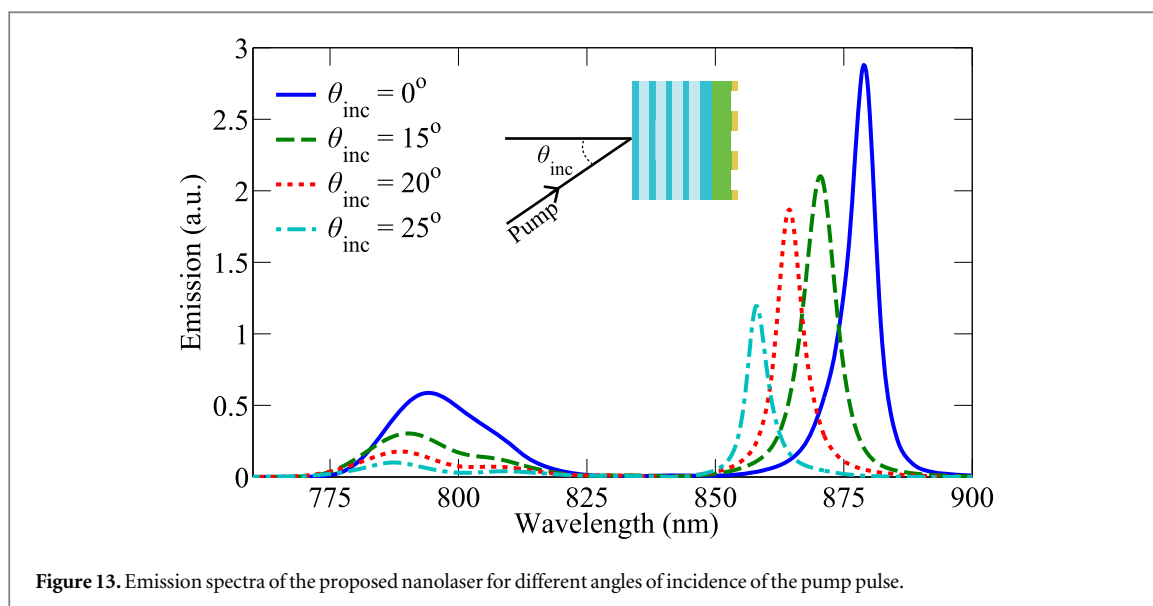
maximum when $d_l = 210$ nm. However, the peak emission intensity decreases as the wavelength corresponding to the peak emission intensity moves away from 870 nm, which is the center of the fluorescence spectra of IR-140 gain medium. As the OTS resonance moves away from 870 nm, the efficiency of energy transfer from the gain medium to plasmonic modes decreases. As a result, we observe a decrease in the lasing emission intensity.

5.2. Gain layer thickness

In figure 12(b), we show the change in the emission spectra when the gain layer thickness, d_g , is varied. We observe that the peak wavelength of lasing emission shifts from 860 nm to 920 nm when d_g is varied from 275 nm to 415 nm. The peak intensity of the emission reaches maximum when the gain medium thickness is ~ 320 nm. When $d_g < 260$ nm or $d_g > 430$ nm, there is an insignificant overlap between the fluorescence spectra of the gain medium and the extinction spectra of the nanoresonator, and therefore, no lasing emission is observed.

5.3. Angle of incidence of pump pulse

In a plasmonic nanolaser, light is confined in a sub-wavelength dimensional gain medium. The light confinement mechanism in a plasmonic nanolaser is different from that in a conventional photonic laser. In a conventional photonic laser, the cavity favors one or more modes within the gain linewidth that resonate in the cavity. The wavelengths of the resonating modes depend on the index contrast between the gain and surrounding media, and the overall dimensions of the cavity. However, in the proposed structure, like in other plasmonic lasers, the wavelength of emission light depends on the plasmonic modes that are excited. The plasmonic modes draw energy from the supporting gain medium for coherent lasing emission [37]. The plasmonic resonance depends on the dimensions of the metal nano-structures rather than on the overall dimensions of the cavity. The plasmonic resonances can also change due to the change in the angle of incident light. There have been several reports of change of the wavelength of Tamm plasmon resonance when the incident light angle changes mainly due to the parabolic dispersive nature of these modes [38–40]. Zhou *et al* showed blue-shift of extinction spectra from 913 nm to 850 nm when the incidence angle changed from zero to



40° in their nanoparticle array-based plasmonic laser [13]. We show that this property can be exploited in our proposed structure to tune the emission wavelength by changing the incidence angle of the pump pulse. Since IR-140 gain medium has a broad gain profile with a linewidth of ~55 nm, the lasing wavelength can be tuned over a broad range with the change of the incidence angle of pump pulse.

Figure 13 presents transmitted spectra when the pump pulse is incident at different angles with transverse-magnetic polarization. When the incident angle is varied from 0° to 25°, the lasing emission shows a blue-shift from 880 nm to 858 nm. Also, as the angle of incidence is increased, the lasing intensity decreases monotonically. We note that the linewidth of the emission does not change significantly as the angle of incidence of the pump pulse varies. We also note that the forward scattering of the pump energy to the emission side decreases as the incidence angle of the pump pulse increases. Transmission spectra remain mostly unchanged when the polarization of the pump pulse changes.

6. Conclusion

In this work, we have presented an efficient plasmonic nanolaser design capable of producing near-infrared narrow-beam emission at room temperature. To design the plasmonic nanocavity, we have chosen square NHA in thin Au layer with subwavelength periodicity. The stimulated emission from the gain medium couples to LSPs in the NHA so that light can be confined in a nanoscale cavity. Due to the subwavelength dimension of the lattice period, only zero-th order diffracted mode exists in the lasing emission under normal incidence. Additionally, we added a 1-D PC on top of the gain medium. The PC was designed to couple the stimulated emission to OTS modes. Therefore, at OTS resonance, light confinement increases significantly near the metal layer, which results in increased coupling to plasmonic modes, and hence increased EOT. Moreover, the PC layers were designed to suppress lasing emission in the backward direction and preferentially guide lasing emission in the forward direction. The proposed design shows ~90% improvement in the transmission intensity compared to that of a structure without PC layers. The proposed nanolaser also suppresses the forward scattering of the pump energy through the NHA by ~80%. Apart from increasing the efficiency of the nanolaser, the 1-D PC also allows us to engineer the lasing emission wavelength. By controlling the thicknesses of gain and PC layers, we can tune the OTS resonance, and hence, the emission peak over ~60 nm. Additionally, the lasing can be tuned over ~20 nm in real-time by changing the angle of incidence of the pump pulse.

ORCID iDs

Muhammad Anisuzzaman Talukder  <https://orcid.org/0000-0002-2814-3658>

References

- [1] Ning C-Z 2010 Semiconductor nanolasers *Physica Status Solidi (b)* **247** 774–88
- [2] Oulton R F, Sorger V J, Zentgraf T, Ma R-M, Gladden C, Dai L, Bartal G and Zhang X 2009 Plasmon lasers at deep subwavelength scale *Nature* **461** 629–32

- [3] Savelev R S, Slobozhanyuk A P, Miroshnichenko A E, Kivshar Y S and Belov P A 2014 Subwavelength waveguides composed of dielectric nanoparticles *Phys. Rev. B* **89** 035435
- [4] Hill M T *et al* 2007 Lasing in metallic-coated nanocavities *Nat. Photon.* **1** 589–94
- [5] Plotz G, Simon H and Tucciarone J 1979 Enhanced total reflection with surface plasmons *JOSA* **69** 419–22
- [6] Sudarkin A and Demkovich P 1989 Excitation of surface electromagnetic waves on the boundary of a metal with an amplifying medium *Sov. Phys. Tech. Phys.* **34** 57
- [7] Seidel J, Grafström S and Eng L 2005 Stimulated emission of surface plasmons at the interface between a silver film and an optically pumped dye solution *Phys. Rev. Lett.* **94** 177401
- [8] Noginov M, Podolskiy V A, Zhu G, Mayy M, Bahoura M, Adegoke J, Ritzo B and Reynolds K 2008 Compensation of loss in propagating surface plasmon polariton by gain in adjacent dielectric medium *Optics Express* **16** 1385–92
- [9] Ma R-M, Oulton R F, Sorger V J, Bartal G and Zhang X 2011 Room-temperature sub-diffraction-limited plasmon laser by total internal reflection *Nat. Mater.* **10** 110–3
- [10] Govyadinov A A and Podolskiy V A 2006 Gain-assisted slow to superluminal group velocity manipulation in nanowaveguides *Phys. Rev. Lett.* **97** 223902
- [11] Ding K and Ning C-Z 2012 Metallic subwavelength-cavity semiconductor nanolasers *Light: Science & Applications* **1** e20
- [12] Berini P and De Leon I 2012 Surface plasmon-polariton amplifiers and lasers *Nat. Photon.* **6** 16–24
- [13] Zhou W, Dridi M, Suh J Y, Kim C H, Co D T, Wasielewski M R, Schatz G C and Odom T W 2013 Lasing action in strongly coupled plasmonic nanocavity arrays *Nat. Nanotechnol.* **8** 506–11
- [14] Symonds C, Lheureux G, Hugonin J P, Greffet J J, Laverdant J, Brucoli G, Lemaitre A, Senellart P and Bellessa J 2013 Confined Tamm plasmon lasers *Nano Letters* **13** 3179–84
- [15] Zhang Z, Li Y, Liu W, Sun Y, Jiang H and Chen H 2016 Lasing effect enhanced by optical Tamm state with in-plane lattice plasmon *J. Opt.* **18** 025103
- [16] van Beijnum F, van Veldhoven P J, Geluk E J, de Dood M J, Gert W and van Exter M P 2013 Surface plasmon lasing observed in metal hole arrays *Phys. Rev. Lett.* **110** 206802
- [17] van Beijnum F, van Veldhoven P J, Geluk E J, W't Hooft G and van Exter M P 2014 Loss compensation of extraordinary optical transmission *Appl. Phys. Lett.* **104** 061112
- [18] Meng X, Liu J, Kildishev A V and Shalaev V M 2014 Highly directional spaser array for the red wavelength region *Laser & Photonics Reviews* **8** 896–903
- [19] Ebbesen T W, Lezec H J, Ghaemi H, Thio T and Wolff P 1998 Extraordinary optical transmission through sub-wavelength hole arrays *Nature* **391** 667–9
- [20] Meng X, Kildishev A V, Fujita K, Tanaka K and Shalaev V M 2013 Wavelength-tunable spasing in the visible *Nano Letters* **13** 4106–12
- [21] Yang A, Hoang T B, Dridi M, Deeb C, Mikkelsen M H, Schatz G C and Odom T W 2015 Real-time tunable lasing from plasmonic nanocavity arrays *Nat. Commun.* **6** 6939
- [22] Yang A, Li Z, Knudson M P, Hryn A J, Wang W, Aydin K and Odom T W 2015 Unidirectional lasing from template-stripped two-dimensional plasmonic crystals *ACS Nano* **9** 11582–8
- [23] Lu Y-J *et al* 2014 All-color plasmonic nanolasers with ultralow thresholds: autotuning mechanism for single-mode lasing *Nano Letters* **14** 4381–8
- [24] Nair L 1982 Dye lasers *Prog. Quantum Electron.* **7** 153–268
- [25] Chang S-H and Taflove A 2004 Finite-difference time-domain model of lasing action in a four-level two-electron atomic system *Optics Express* **12** 3827–33
- [26] Taflove A and Hagness S C 2005 *Computational Electrodynamics* (Boston, MA: Artech house)
- [27] Johnson P B and Christy R-W 1972 Optical constants of the noble metals *Phys. Rev. B* **6** 4370
- [28] Melentiev P, Afanasiev A, Kuzin A, Zablotskiy A, Baturin A and Balykin V 2011 Single nanohole and photonic crystal: wavelength selective enhanced transmission of light *Optics Express* **19** 22743–54
- [29] Leon I D and Berini P 2010 Amplification of long-range surface plasmons by a dipolar gain medium *Nat. Photon.* **4** 382–7
- [30] Van der Molen K, Koerkamp K K, Segerink F, Van Hulst N, Enoch S and Kuipers L 2005 Shape resonances in extraordinary transmission *Quantum Electronics Conference* (Piscataway, NJ: IEEE) pp 339
- [31] Van der Molen K, Koerkamp K K, Enoch S, Segerink F, Van Hulst N and Kuipers L 2005 Role of shape and localized resonances in extraordinary transmission through periodic arrays of subwavelength holes: experiment and theory *Phys. Rev. B* **72** 045421
- [32] Treshin I V, Klimov V V, Melentiev P N and Balykin V I 2013 Optical tamm state and extraordinary light transmission through a nanoaperture *Phys. Rev. A* **88** 023832
- [33] Zhou H, Yang G, Wang K, Long H and Lu P 2010 Multiple optical Tamm states at a metal-dielectric mirror interface *Opt. Lett.* **35** 4112–4
- [34] Zhang X-L, Song J-F, Li X-B, Feng J and Sun H-B 2013 Strongly localized evanescent optical tamm states at metal-DBR interface *J. Lightwave Technol.* **31** 1654–9
- [35] Palik E D 1998 *Handbook of Optical Constants of Solids* (Edinburgh: Academic Press)
- [36] Sasin M *et al* 2010 Tamm plasmon-polaritons: first experimental observation *Superlattices Microstruct.* **47** 44–9
- [37] Zheludev N I, Prosvirnin S L, Papasimakis N and Fedotov V A 2008 Lasing spaser *Nat. Photon.* **2** 351–4
- [38] Huang Y-S, Hu S-Y, Huang C-C, Lee Y-C, Lee J-W, Chang C-C, Wun Z-K and Tiong K-K 2014 Incident-angle-dependent reflectance in distributed Bragg reflectors fabricated from ZnO/MgO multilayer films *Opt. Rev.* **21** 651–4
- [39] Kavokin A, Shelykh I and Malpuech G 2005 Lossless interface modes at the boundary between two periodic dielectric structures *Phys. Rev. B* **72** 233102
- [40] Kaliteevski M, Iorsh I, Brand S, Abram R, Chamberlain J, Kavokin A and Shelykh I 2007 Tamm plasmon-polaritons: possible electromagnetic states at the interface of a metal and a dielectric Bragg mirror *Phys. Rev. B* **76** 165415